Atypical, but not typical, antipsychotic drugs reduce hyper-synchronized prefrontal-hippocampal circuits during psychosis-like states in mice: contribution of 5-HT2A and 5-HT1A receptors

Cristina Delgado-Sallent[1], Pau Nebot[1], Thomas Gener[1], Amanda B Fath[1,2], Melina Timplalexi[1], and M. Victoria Puig[1]

[1] Hospital del Mar Medical Research Institute, Barcelona Biomedical Research Park, 08003 Barcelona, Spain

[2] Department of Brain and Cognitive Sciences, Massachusetts Institute of Technology, Cambridge, MA, 02139 USA

Correspondence: M. Victoria Puig (mpuig3@imim.es)

Keywords: schizophrenia, NMDA antagonist, risperidone, clozapine, haloperidol

ABSTRACT

Neural synchrony and functional connectivity are disrupted in schizophrenia. We investigated changes in prefrontal-hippocampal neural dynamics during psychosis-like states induced by the NMDAR antagonist phencyclidine and subsequent rescue by two atypical antipsychotic drugs (AAPDs), risperidone and clozapine, and the classical APD haloperidol. The psychotomimetic effects of phencyclidine were associated with prefrontal hypersynchronization, hippocampal desynchronization and disrupted circuit connectivity. Phencyclidine boosted prefrontal oscillatory power at atypical bands within delta, gamma, and high frequency ranges while irregular cross-frequency and spike-LFP coupling emerged. In the hippocampus phencyclidine enhanced delta rhythms, but suppressed theta oscillations, theta-gamma coupling, and theta-beta spike-LFP coupling. Baseline inter-regional theta-gamma coupling, theta phase coherence, and hippocampus-to-cortex theta signals were redirected to delta frequencies. Risperidone and clozapine, but not haloperidol, reduced phencyclidine-induced prefrontal and cortical-hippocampal hypersynchrony. None of the substances restored hippocampal and circuit desynchronization. These results suggest that AAPDs, but not typical APDs, target prefrontal-hippocampal pathways to elicit antipsychotic action. We investigated whether the affinity of AAPDs for serotonin receptors could explain their distinct effects. Serotonin 5-HT_{2A}R antagonism by M100907 and 5-HT_{1A}R agonism by 8-OH-DPAT reduced prefrontal hypersynchronization. Our results point to fundamentally different neural mechanisms underlying the action of atypical versus typical APDs with selective contribution of serotonin receptors.

INTRODUCTION

Disruption of neural synchrony and spatio-temporal communication in brain circuits involving the prefrontal cortex (PFC) and the hippocampus (HPC) is considered a hallmark characteristic of neuropsychiatric disorders such as schizophrenia (Godsil et al. 2013; Baker et al. 2014; Sigurdsson and Duvarci 2016). Patients with schizophrenia exhibit irregular gamma oscillatory activities (>25 Hz) in cortical regions that have been associated with positive symptoms, such as hallucinations (Spencer et al. 2008, 2009; Uhlhaas and Singer 2010; Grützner et al. 2013), and display disrupted functional connectivity within prefrontal-hippocampal circuits that correlate with poor executive function (Benetti et al. 2009; Minzenberg et al. 2009; Heckers and Konradi 2010; Sigurdsson and Duvarci 2016). Rodent models used to study schizophrenia also show prefrontal-hippocampal dysfunction, including increased power in gamma oscillations and high frequency oscillations (HFOs, >100 Hz) (Hunt and Kasicki 2013; Jodo 2013) and reduced circuit synchrony (Sigurdsson et al. 2010; Sigurdsson 2016). Hypofunction of the N-Methyl-D-aspartate receptors (NMDARs) has also been proposed to be an important factor in the pathophysiology of schizophrenia. NMDAR antagonists are used to model schizophrenia in humans and animals mimicking some of the core positive, negative, and cognitive symptoms of the disorder. For example, acute administration of the NMDAR antagonist ketamine produces transient psychotic-like symptoms in healthy people while it exacerbates pre-existing symptoms in schizophrenia patients (Krystal et al. 1994; Lahti et al. 1995). In rodents, acute NMDAR antagonism mediated by phencyclidine (PCP) or ketamine generates atypical behaviors, such as increased locomotor activity, stereotyped behaviors and ataxia, associated with the positive symptoms of schizophrenia (Sturgeon et al. 1979). These behaviors correspond with irregular gamma oscillatory activities and increased power of HFO across different brain regions (Hunt et al. 2006, 2015). However, alterations in connectivity within prefrontal-hippocampal circuitry in the psychotic-like states induced by NMDAR antagonists is unresolved.

Antipsychotic drugs (APDs) are classified as classical and atypical based on their affinities for dopamine and serotonin receptors. Atypical APDs primarily bind to serotonin receptors and have been shown to ameliorate cognitive and negative symptoms in addition to psychosis in schizophrenia patients and animal models of NMDAR hypofunction (Meltzer and McGurk 1999; Grayson et al. 2007; Houthoofd et al. 2008; Neill et al. 2010). Classical APDs like haloperidol primarily block dopamine D2 receptors (D2Rs) and weakly bind to serotonin receptors, which in turn has shown to be less effective in the recovery of cognitive and negative symptoms (Meltzer and Huang 2008; Meltzer and Massey 2011). Serotonin 1A (5-HT_{1A}Rs) and 2A (5-HT_{2A}Rs) receptors are major targets for atypical APDs such as risperidone or clozapine. The PFC and HPC densely express both serotonin receptors (Puig and Gulledge 2011; Berumen et al. 2012; Celada et al. 2013; Puig and Gener 2015), whereas D2R are moderately present (Santana et al. 2009; Puighermanal et al. 2015). Therefore, atypical APDs binding to serotonin receptors are expected to have major effects on prefrontal-hippocampal neural dynamics.

We have recently shown that risperidone reduces local and cross-regional synchronization of prefrontal-hippocampal circuits in mice under normal conditions, with 5-HT_{1A}R, 5-HT_{2A}R and D2R shaping distinct frequency bands (Gener et al. 2019). Here we investigate the neural dynamics of prefrontal-hippocampal circuits under the psychotomimetic conditions produced by an acute dose of PCP. We further explore the ability of the APDs risperidone, clozapine, and haloperidol, the 5-HT_{2A}R antagonist M100907 and the 5-HT_{1A}R agonist 8-OH-DPAT to rescue the circuit dysfunction produced by PCP. We hypothesized that the serotonergic component, but not the dopaminergic component, of atypical APDs plays a relevant role in their modulation of prefrontal-hippocampal activity during psychosis.

MATERIALS AND METHODS

Animals. Thirty adult male C57BL/6 mice 2 to 3 months old were used. All procedures were conducted in compliance with EU directive 2010/63/EU and Spanish guidelines (Laws 32/2007, 6/2013 and Real Decreto 53/2013) and were authorized by the Barcelona Biomedical Research Park (PRBB) Animal Research Ethics Committee and the local government.

Behavioral assessment. Changes in locomotion, stereotypic behaviors and ataxia were investigated using video recordings with a PointGrey Camera. Quantification of these behavioral measures were performed in 10-minute windows during the baseline condition and after the administration of PCP. Locomotion was calculated using the MouseActivity software (Zhang et al. 2020). Stereotypic behaviors and ataxia were rated using a custom scale from 0 to 5 based on previous literature (Sturgeon et al. 1979). Scales were adapted to the electrophysiological recordings considering the influence of the cable and implant. Stereotypic behaviors were rated as follows: 0: Non-repetitive activity; 1: Small rate of weaving, more locomotion, sniffing and grooming; 2: Moderate weaving, non-directed movements and rearing; 3: Fast and frequent weaving and intermittent turning; 4: Rapid rate and continuous turning and weaving; 5: Dyskinetic extension and flexion of the limbs. Ataxia rates: 0: Coordinated movement; 1: Small rate of unusual movement and loss of balance during rearing; 2: Moderate rate of unusual movements and falling, may support weight on the abdomen while moving; 3: Constant rearing with loss of balance and falling, moderate support of weight in the abdomen while moving; 4: Cannot move from a restricted area and supports weight on the abdomen while not moving; 5: Unable to move or convulsive movements.

Surgeries. Mice were induced with a mixture of ketamine/xylazine and placed in a stereotaxic apparatus. Anesthesia was maintained with continuous 0.5-4% isoflurane. Small craniotomies were drilled above the medial PFC and HPC. Several micro-screws were screwed into the skull to stabilize the implant, and the one on top of the cerebellum was used as a general ground. Three tungsten electrodes, one stereotrode and one single electrode, were implanted in the prelimbic region of the medial PFC and two more were

implanted in the CA1 area of the HPC. The electrodes were positioned stereotaxically in the prelimbic (AP: 1.5, 2.1 mm; ML: ± 0.6, 0.25 mm; DV: -1.7 mm from bregma) and CA1 (AP: -1.8, -2.5 mm; ML: -1.3, -2.3 mm; DV: -1.15, -1.25 mm) areas. Neural activity was recorded while the electrodes were being lowered down inside the brain to help locate the CA1 region. In addition, three reference electrodes were implanted in the corpus callosum and lateral ventricles (AP: 1, 0.2, -1; ML: 1, 0.8, 1.7; DV: -1.25, -1.4, -1.5, respectively). The electrodes were made with two twisted strands of tungsten wire 25 μm wide (Advent, UK) and were held together using heat insulation. At the time of implantation, the electrodes had an impedance from 100 to 400 kOhm and were implanted unilaterally with dental cement. Electrode wires were pinned to an adaptor to facilitate their connection to the recording system. After surgery, animals were allowed at least one week to recover during which they were extensively monitored and received both analgesia and anti-inflammatory treatments. Additionally, animals were handled and familiarized with the implant connected to the recording cable. After the experiments ended, the electrode placements were confirmed histologically by staining the brain slices with Cresyl violet (Supplementary Fig. 1). Electrodes with tips outside the targeted areas were discarded from data analyses.

Neurophysiological recordings and data analyses. All the recordings were implemented with the multi-channel Open Ephys system at 0.1-6000 Hz and a sampling rate of 30 kHz. Recorded signals from each electrode were filtered offline to extract local field potentials (LFPs), single-unit activity (SUA), and multi-unit activity (MUA). To obtain LFPs, recorded signals were detrended, notch-filtered and decimated to 1kHz offline. The frequency bands considered for the band-specific analyses included: delta (2-5 Hz), fast delta (4-8 Hz), theta (8-12 Hz), alpha (10-14 Hz), beta (18-25 Hz), low gamma (30-48 Hz), high gamma (52-100 Hz), and HFOs (100-200 Hz). Neural signals were analyzed in one-minute windows and averaged across 10 minute epochs during baseline and after drug administration. Power spectral density results were calculated using the multi-taper method. Spectrograms were constructed using consecutive Fourier transforms. Phase-amplitude coupling (PAC) was measured following the method described in Tort et al. (Tort et al. 2008). The parameters used were: phase frequencies = [0, 15] with 1 Hz step and 4 Hz

bandwidth, amplitude frequencies = [10, 250] with 5 Hz step and 10 Hz bandwidth. The length of the sliding window was 300s for the overview plots and 60s for the quantifications, with no overlap. PAC quantification results were obtained by averaging the values of selected areas of interest in the comodulograms. Prefrontal-hippocampal phase coherence was estimated via the weighted phase-lag index (wPLI), a measure of phase synchronization between areas aimed at removing the contribution of common source zero-lag effects that allowed us to estimate the synchronization between the PFC and the HPC mitigating source signals affecting multiple regions simultaneously (Stam et al. 2007; Vinck et al. 2011; Hardmeier et al. 2014; Gener et al. 2019). wPLI color plots were built by applying the previous function multiple times in 1Hz-60s sliding windows (Butterworth bandpass filters of order 3) with no overlap. LFP power, PAC and wPLI are provided as z-scores with respect to baseline (data is demeaned by the baseline mean and then normalized by the baseline standard deviation). Directionality of signals between areas was calculated with the phase slope index (PSI) with a Python translation of MATLAB's data2psi.m (epleng = 60s, segleng = 1s) as in reference (Nolte et al. 2008). PSI color plots were constructed with the same strategy as the wPLI plots but using a 2 Hz sliding window. MUA was estimated by first subtracting the raw signal from each electrode with the signal from a nearby referencing electrode to remove artifacts related to the animal's movement. Then, continuous signals were filtered between 450-6000 Hz with Python and thresholded at -3 sigma standard deviations with Offline Sorter v4 (Plexon Inc.). From the MUA we sorted the spikes into individual neurons to obtain SUAs. We estimated MUA and SUA in 1-minute non-overlapping windows. Spike-LFP coupling was estimated with the pairwise phase consistency (PPC) method, which is an unbiased parameter to determine the degree of tuning of the neurons' firing to ongoing network activity at specific frequencies (Vinck et al. 2011; Zorrilla de San Martin et al. 2020). PPC was determined using the phases of 1000 spikes from MUA, only considering epochs with at least 250 spikes. We used the instantaneous module of the raw x, y and z signals from the accelerometer (Acc) to evaluate the effects of the drugs on general mobility of mice as in previous studies (Gener et al. 2019; Alemany-González et al. 2020).

Pharmacology. The doses used were: phencyclidine (PCP) 10 mg/kg; risperidone (RIS) 0.5 mg/kg; clozapine (CLZ) 1 mg/kg; haloperidol (HAL) 0.5 mg/kg; M100907 1 mg/kg; 8-OH-DPAT (DPAT) 1 mg/kg (Gener et al. 2019). PCP and the corresponding saline controls were administered subcutaneously (SC) whereas the rest of the drugs were administered intraperitoneally (IP). Twenty-four animals were used in two experiments and six mice were used in three experiments. We left at least one week between experiments for proper washout of the drugs.

Statistical analyses. One-way repeated measures ANOVA (parametric or nonparametric) was used to test for statistical significance with time as within subject factor (e.g., baseline, saline, PCP, and drug) for Acc, behavior, power, PAC, wPLI, PSI, SUA, MUA, and PPC. Additionally, two-way repeated measures ANOVA was used to test for statistical significance with treatment as between factor (PCP+saline vs. saline controls and PCP+saline vs. PCP+drug) and time as within subject factor (baseline, saline, PCP, and drug). Statistical analyses were conducted using raw data in Python with the Pingouin statistical package (Vallat 2018).

RESULTS

Acute NMDAR antagonism boosts prefrontal synchronization, desynchronizes the hippocampus, and disrupts circuit connectivity

We investigated how acute NMDAR antagonism influences behavior and neural activity in the prelimbic PFC and the CA1 region of the HPC. To elicit psychotomimetic conditions, we administered PCP acutely (10 mg/kg, SC) in freely moving mice. This dose of PCP induces strong psychotic-like behaviors in mice, such as hyperlocomotion, stereotypies and ataxia, that can be mostly treated with APDs (Sturgeon et al. 1979; Castañé et al. 2015; Lee et al. 2017). We first aimed to validate this model of psychosis in our experimental conditions where mice were connected to an electrophysiological data acquisition system via

an electrical cable. Mice received PCP followed by saline or risperidone (0.5 mg/kg, IP) fifteen minutes after PCP administration. Mice were given one week of washout between each experimental condition. As expected, PCP increased locomotor activity (distance traveled) and stereotypies that were greatly reduced by risperidone (n = 4 mice; two-way ANOVA with time as within factor and drug combination as between factor; interaction: $F_{7,42}$ = 10.35, 2.59, p < 0.0005, 0.03; Fig. 1a,b). In contrast, PCP-mediated ataxia was exacerbated by risperidone in an initial phase ($F_{7,42}$ = 23.16, p < 0.005) and then followed PCP's pattern (Fig. 1b). The PCP-induced and risperidone-induced behaviors were reflected as partial and large reductions of accelerometer rates, respectively, that were recorded via the accelerometer integrated within the headstages of the electrophysiological system ($F_{8,64}$ = 9.44, 2.29, p < 0.0005, 0.031; Fig. 1c). We harnessed these changes in accelerometer rates to assess PCP-induced and APD-induced behaviors over time in the subsequent pharmacological experiments described below.

In a different cohort of animals, we examined the time course of PCP's effects on prefrontal-hippocampal neural dynamics at 15, 30 and 60 minutes after PCP administration (n = 9 mice) compared to saline administration (n = 10 mice; Fig. 2a and Supplementary Fig. 2). Again, PCP induced hyperlocomotion, stereotypies and ataxia that partially reduced the accelerometer rates ($F_{1,8}$ = 16.73, p <0.0005). The atypical behaviors induced by PCP were accompanied by substantial alterations in neural oscillations that could be readily seen in the unprocessed local field potentials (Fig. 2b). Several aberrant bands emerged in the PFC after injection of PCP: a wide band from 1 to 8 Hz that included the standard "slow" delta (2-5 Hz) and an atypical "fast" delta band (4-8 Hz, peak at 6.4 ± 0.2 Hz), a theta band (8.3 ± 0.1 Hz), an alpha band (10-14 Hz, peak at 10.2 ± 0.06 Hz), a narrow band within the high gamma range (40-75 Hz, peak at 60.3 ± 1.1 Hz), and broadly increased HFOs (100-200 Hz) that included a prominent band between 140-180 Hz (peak at 160.5 ± 2.54 Hz; $F_{1,8}$ = 21.4, 22.73, 20.07, 13.67, 17.31 and 17.93, respectively; p <0.0005, one-way ANOVA; significant differences with saline controls; Fig. 2c,d). These bands appeared *de novo* and revealed strong hypersynchronization of prefrontal microcircuits by PCP. In the HPC, the power changes were modest and mostly differed from the PFC, except for the delta band that closely followed the pattern

found in the PFC ($F_{1,8}$ = 20.07, p <0.0005). PCP decreased the power of hippocampal theta (8-12 Hz) and beta (18-25 Hz) oscillations with respect to baseline ($F_{1,8}$ = 14.6, 23.53, p = 0.002, <0.0005) and increased high gamma oscillations in a band that appeared earlier and was shorter than in the PFC (the first 15 min only; $F_{1,8}$ = 18.2, p < 0.0005; Fig. 2c).

To further assess local and circuit synchronization we quantified cross-frequency phase-amplitude coupling (PAC) between slow rhythms (2-16 Hz) and faster oscillations (50-250 Hz) (Jensen and Colgin 2007; Scheffer-Teixeira and Tort 2017). PAC was investigated both within the PFC and the HPC (local PAC or l-PAC: PFC_{phase}-PFC_{amp} and HPC_{phase}-HPC_{amp}) and at the circuit level via coupling of HPC phase with PFC amplitude and vice versa (inter-regional PAC or ir-PAC: HPC_{phase}-PFC_{amp} and PFC_{phase}-HPC_{amp}). Overall, changes in cross-frequency coupling corresponded with the power increases and decreases observed in the PFC and HPC, respectively. First, PCP promoted fast delta-HFO coupling within the PFC and delta-HFO HPC_{phase}-PFC_{amp} coupling within the circuit ($F_{1,8}$ = 21, 18.77, p < 0.0005, 0.002; Fig. 2e). As reported previously (Hentschke et al. 2007; Colgin 2015; Scheffer-Teixeira and Tort 2017), theta-gamma coupling within the CA1 region was present during baseline periods, with phases varying from 5 to 12 Hz and amplitude frequencies varying from 50 to 100 Hz (Fig. 2e). After PCP, this theta-gamma coordination rapidly subsided ($F_{1,8}$ = 23.13, p < 0.0005). At a circuit level, we found that the phase of PFC theta modulated the amplitude of CA1 high gamma (PFC_{phase}-HPC_{amp}), as reported recently (Zhang et al. 2016; Nandi et al. 2019; Tavares and Tort 2020). As observed in the HPC, PCP weakened this circuit coupling ($F_{1,8}$ = 17.4, p = 0.0006; Fig. 1e).

We next investigated whether PCP altered the interaction between brain areas. We first examined prefrontal-hippocampal phase coherence via the weighted phase-lag index (wPLI) method (Vinck et al. 2011; Hardmeier et al. 2014). In accordance with the power increases observed in the PFC, PCP generated circuit hypersynchronization at high frequencies (HFO wPLI: $F_{1,8}$ = 12.87, p = 0.005; milder increases at low and high gamma). In addition, PCP desynchronized circuit coherence at middle frequencies (theta, alpha and beta wPLI: $F_{1,8}$ = 21, 8.07, 14.47, p <0.0005, 0.044 and 0.002, respectively; significant differences

with saline controls). In fact, theta coherence shifted to fast delta (peak from 8.45 ± 0.15 to 6.36 ± 0.43 Hz) for at least 30 min after PCP injection (Fig. 2f). We also quantified the directionality of the signals between the PFC and the HPC via the phase slope index (PSI) (Nolte et al. 2008). During baseline, a strong flow of information at theta frequencies originated in the HPC and traveled to the PFC. In accordance with changes in phase coherence, PCP disrupted theta directionality ($F_{1,8}$ = 4.04, p = 0.018) and generated an aberrant flow of information between 3 and 6 Hz (delta) from the PFC to the HPC ($F_{1,8}$ = 3.4, p = 0.034; Fig. 2g).

We finally examined whether PCP modified the firing rate of neurons and their synchronization to ongoing neural oscillations. PCP did not produce significant changes in the firing rate of individual neurons (SUA) or population activity (MUA) in either brain region (20 and 15 isolated neurons in the PFC and HPC, respectively, from 5 mice; Fig. 2h). However, it induced many alterations in the synchronization of spikes with ongoing oscillations. This was assessed via the pairwise phase consistency (PPC) method, which estimates the phase coupling of spikes to different oscillatory bands. The phase-locking of spikes to low and high gamma oscillations was more robust in the PFC after PCP (n = 5 mice; $F_{1,4}$ = 9.24, 7.8, p = 0.026, 0.05). Phase-locking to delta oscillations in the PFC was also partially increased by PCP. In the HPC, there was an initial increase in spike-LFP coupling to high gamma oscillations, closely following the short increase in high gamma power ($F_{1,4}$ = 10.2, p = 0.017), whereas phase-locking to theta, beta and low gamma decreased ($F_{1,4}$ = 9, 10.68, 9.72, p = 0.029, 0.014, 0.021; Fig. 2i). No major changes in spike-LFP coupling were observed at higher frequencies in either region.

Altogether, the abnormal power, cross-frequency coupling, and spike-LFP coupling unraveled a strong hypersynchronization of cortical microcircuits by PCP while hippocampal microcircuits became desynchronized. Moreover, a delta drive was observed in both areas. Finally, the circuit's connectivity was severely disrupted by PCP.

Partial rescue of phencyclidine-induced impaired prefrontal-hippocampal neural dynamics by atypical, but not typical, antipsychotic drugs

We next investigated the individual fingerprints of antipsychotic action on PCP-induced neurophysiological alterations by the atypical APDs risperidone and clozapine and the classical APD haloperidol. Fifteen minutes after the administration of PCP, one of the three APDs was administered. We compared the neural signals recorded at 15 and 45 min after APD injection (30 and 60 min after PCP injection) with a control group that only received saline (PCP+SAL, n = 6 mice, Supplementary Fig. 2). In these experiments, additional control injections with saline were performed before the administration of PCP.

Risperidone (RIS, 0.5 mg/kg; n = 7 mice) reduced the hyperlocomotion and stereotypies produced by PCP and left the mice in a sedative state that caused immobility (Acc: $F_{1,6} = 23.82$, $p < 0.0005$, one-way ANOVA; [PCP+SAL vs. PCP+RIS] $F_{2,22} = 4.33$, $p = 0.026$, two-way ANOVA; Fig. 1) and a strong inhibition of neural activity. More specifically, risperidone decreased PCP-associated power enhancement at theta, high gamma and HFO in the PFC ($F_{2,22} = 3.64, 9.99, 5.75$, $p = 0.043, 0.0008, 0.01$, respectively; Fig. 3a,b) and further reduced theta oscillations in the HPC ($F_{2,22} = 4.55$, $p = 0.056$). However, narrow bands in the high gamma and HFO domains continued in the PFC, steadily decreasing their frequency over time. Concomitantly, the main delta frequencies shifted from fast to slower ranges in both brain regions (PFC: peak from 6.4 to 3.7 Hz; HPC: peak from 6.01 to 3.67 Hz; Fig. 3b). We next investigated the actions of clozapine on PCP-mediated changes in behavior and oscillatory power. Clozapine (CLZ, 1 mg/kg; n = 6 mice) reduced behavioral alterations and power increases, however caused fewer suppressive effects than risperidone. First, it decreased general mobility of mice ($F_{1,5} = 6.82$, $p = 0.004$, one-way ANOVA; [PCP+SAL vs. PCP+CLZ] $F_{2.20} = 4.93$, $p = 0.051$, two-way ANOVA), but less than risperidone ([PCP+CLZ vs PCP+RIS] $F_{2.22} = 6.28$, $p = 0.005$). Moreover, it slightly decreased amplified high gamma in the PFC ($F_{2,22} = 4.46$, $p = 0.066$) but, unlike risperidone, it was unable to reduce the increased theta and HFOs. In addition, fast delta partially shifted to slow delta in both regions: two peaks at 5.05 and 3.14 Hz were

observed in the PFC whereas in the HPC the band shifted from 6.01 to 3.47 Hz (Fig. 3c; insignificant changes in slow and fast delta power). We subsequently examined the effects of the classical APD haloperidol (HAL, 0.5 mg/kg; n = 5 mice). The general mobility of the mice after the administration of haloperidol was like the control group ([PCP+SAL vs. PCP+HAL] $F_{2,18} = 0.26$, $p = 0.77$), and above that of the risperidone group ([PCP+HAL vs. PCP+RIS] $F_{2,18} = 7.31$, $p = 0.004$). This suggests that administration of haloperidol did not induce major sedative effects. Notably, haloperidol was unable to block the aberrant fast delta, theta, high gamma and HFO bands elicited by PCP in the PFC (Fig. 3d). Clozapine and haloperidol did not restore intrinsic theta and beta oscillations in the HPC.

We then examined whether the three antipsychotic drugs rescued abnormal local and inter-regional cross-frequency coupling produced by PCP. Risperidone decreased the frequency of the newly generated fast delta-HFO l-PAC and ir-PAC that emerged in the PFC (PCP+SAL vs. PCP+RIS]; $F_{2,22} = 5.73, 5.14$, $p = 0.001, 0.014$; Fig. 4a,b). However, clozapine and haloperidol could not suppress this new coupling (Fig. 4c,d). None of the compounds rescued the inherent theta-gamma coupling in the HPC or the circuit. We next investigated the effects of the compounds on the circuit communication via phase coherence and directionality of signals. Risperidone reduced the circuit's hypersynchronization at HFOs ($F_{2,22} = 4.25$, $p = 0.027$), but not the ones at fast delta or high gamma (Fig. 5a,b). Clozapine only partially reduced high gamma and HFO hypersynchronization but blocked enhanced coherence at fast delta ($F_{2.22} = 5.62$, $p = 0.039$; Fig. 5c). Haloperidol did not correct the augmented coherence at delta, high gamma and HFOs, which remained similar to saline controls (Fig. 5d). None of the APDs rescued the low theta-beta coherence produced by PCP. We subsequently assessed how the three drugs modulated the flow of information within the circuit. Risperidone had no major effects on the aberrant PFC-to-HPC delta signals compared to the saline group (Fig. 5a,b). In contrast, clozapine prevented the emergence of PFC-to-HPC delta signals ($F_{1,16} = 5.2$, $p = 0.045$) and promoted a HPC-to-PFC theta drive resembling that observed during baseline (Fig. 5c). The abnormal PFC-to-HPC delta drive was in fact exacerbated by haloperidol with respect to the control group ([PCP+HAL vs. PCP+SAL] $F_{1,9} = 8.42$, $p = 0.018$; Fig. 5d).

We finally examined whether the compounds affected the firing rate and the abnormal spike-LFP coupling observed after PCP. Risperidone reduced the firing rate of individual neurons in both brain regions ([PFC, HPC] $F_{2,12}$ = 6.66, 8.33, p = 0.011, 0.005) whereas clozapine and haloperidol left spiking activity unchanged (Fig. 6a,b,c). Both risperidone and clozapine partially restored PCP-enhanced delta and high gamma spike-LFP coupling in the PFC ($F_{2,14}$ = 4.47, p = 0.031), but not low gamma coupling. Finally, haloperidol corrected the enhanced delta phase-locking in the PFC ($F_{2,14}$ = 5.69, p = 0.018) but was unable to rescue increased low and high gamma coupling. None of the ADPs restored the suppressed spike-LFP coupling at theta, beta, and low gamma in the HPC.

To disentangle the antipsychotic and sedative effects of the atypical APDs, we conducted further experiments where we administered risperidone and clozapine without PCP. Risperidone caused sedation but it was accompanied by a mild circuit inhibition (Supplementary Fig. 3) whereas clozapine's behavioral and neurophysiological effects were negligible (Supplementary Fig. 4). Therefore, the rescue of PCP's alterations by both compounds were likely antipsychotic in nature. Exceptionally, risperidone disrupted the circuit directionality, which may have influenced its inability to restore the theta flow of information after PCP. Haloperidol did not rescue PCP's alterations. We note that the dose of haloperidol used was medium to high as it inhibited the circuit when administered alone (Gener et al. 2019). Thus, the dose used was not the main cause of its limited efficacy. In brief, risperidone and clozapine reduced PCP-induced prefrontal and cortical-hippocampal hypersynchrony, whereas the main antipsychotic effects of haloperidol were likely independent from prefrontal-hippocampal circuits.

Serotonin receptors 5-HT_{2A} and 5-HT_{1A} play complementary roles in shaping prefrontal-hippocampal neural dynamics during psychosis-like states

Risperidone and clozapine block 5-HT_{2A}Rs directly and stimulate 5-HT_{1A}Rs indirectly (Meltzer and Massey 2011; Celada et al. 2013). We investigated the abilities of a 5-HT_{2A}R antagonist and a 5-HT_{1A}R agonist to rescue PCP-induced effects to gain further insight into the serotonergic component of the two atypical APDs. The selective 5-HT_{2A}R antagonist M100907 (1 mg/kg; n = 6 mice) produced strong sedative effects that caused the animals to become immobile (Acc $F_{1,5}$ = 57.47, p <0.0005, one-way ANOVA; $F_{2,20}$= 10.2, p = 0.01, two-way ANOVA). Concomitantly, it reduced PCP-generated bands in the PFC (theta, alpha, high gamma, HFOs: $F_{2,20}$ = 6.39, 5, 12.06, 9.98, p = 0.007, 0.017, 0.0003, 0.01; two-way ANOVA; Fig. 7a,b). Narrow bands in the gamma domain remained in both structures, while prefrontal HFO also decreased in frequency, following similar temporal patterns compared to risperidone. Also concurrent with risperidone, M100907 shifted the power of fast delta and fast delta-HFO coupling towards slower frequencies. In the HPC, M100907 did not rescue the sharp theta and beta power decreases. Notably, the intrinsic hippocampal and circuit theta-gamma coupling changed to delta-high gamma coupling (2-5 to 50-80 Hz; $F_{2,18}$ = 9.17, 6.18, p = 0.009, 0.035; Fig. 6c). M100907 also partly normalized circuit phase hypersynchronization at gamma and HFOs ($F_{2,18}$ = 10.34 6, p = 0.0010, 0.036; Fig. 7d), however the reduction of theta, alpha and beta coherence was further increased ($F_{1,9}$ = 17.8, 11.99, 2.8 p = 0.002, 0.0005, 0.087). Moreover, M100907 shifted fast delta to slow delta phase synchronization. The intrinsic HPC-to-PFC theta directionality was not restored and the PFC-to-HPC fast delta band not prevented by M100907 (Fig. 7e). In addition, M100907 reduced the firing rate of neurons in the PFC and the HPC ($F_{4,14}$ = 4.04, p = 0.027, one-way ANOVA; [HPC] $F_{2,14}$ = 4.42, p = 0.032, two-way ANOVA) and shifted the spike-LFP coupling from high gamma to low gamma in the PFC, closely following power changes at the same frequencies (Fig. 7f, g). Finally, the PCP-induced increase in delta spike-LFP coupling was partially reduced by M100907. In the HPC, M100907 was unable to restore the changes in spike-LFP coupling at theta and beta. Overall, 5-HT_{2A}R antagonism exerted very similar effects to risperidone.

Lastly, we investigated the effects of the selective 5-HT_{1A}R agonist DPAT (1 mg/kg; n = 6 mice). Mice mobility was reduced much less by DPAT than by M100907 ($F_{1,5}$ = 4.38, p = 0.021, one-way ANOVA; $F_{2,26}$ = 0.83, p = 0.44, two-way ANOVA; [PCP+DPAT vs PCP+M100907] $F_{2,20}$ = 5.66, p = 0.011), suggesting no sedative effects. DPAT rescued abnormal power in both brain regions, although it had less influence on prefrontal neural activities than M100907. More specifically, DPAT decreased the power of high gamma and HFOs in the PFC ($F_{2,26}$ = 7.79, p = 0.002; Fig. 8a,b) but it was unable to reduce the enhanced theta and alpha bands. In addition, there was a partial transition from fast to slow delta power in both regions. DPAT rescued increased fast delta-HFO coupling ($F_{2,26}$ = 2.68, 4.57, p = 0.087, 0.002) but baseline theta-gamma coupling was not restored (Fig. 8c). Moreover, 5-HT_{1A}R agonism had little effect on phase coherence and circuit directionality (Fig. 8d,e). Similar to M100907, DPAT reduced firing rate in both brain regions ($F_{2,14}$ = 12.48, 10.69, p = 0.014, 0.002) and shifted enhanced spike-LFP coupling from high gamma to slower frequencies in the PFC (Fig. 8f,g). However, DPAT was unable to restore the changes in delta coupling in the PFC and theta-beta-gamma coupling in the HPC.

DISCUSSION

We found that the psychotomimetic effects of PCP were associated with hypersynchronization of the PFC, desynchronization of the HPC and disrupted communication of prefrontal-hippocampal pathways. In the PFC, PCP boosted oscillatory power at atypical frequencies within delta, gamma, and high frequency ranges, generated delta-HFO coupling, and enhanced spike-LFP coupling at gamma that suggested the presence of hypersynchronous cortical microcircuits. In the HPC, PCP enhanced delta rhythms, but suppressed theta oscillations, theta-gamma coupling, and theta-beta spike-LFP coupling. Intrinsic inter-regional theta-gamma coupling, theta phase coherence and hippocampus-to-cortex theta signals were redirected to cortex-to-hippocampus delta frequencies.

Prefrontal-hippocampal circuits were initially governed by fast delta rhythms following the administration of PCP. The circuit later transitioned into a state dominated by aberrant rhythms at higher frequencies while the delta drive was attenuated. These events disrupted the normal function of the circuit, weakening inherent hippocampal theta oscillations, theta-gamma coupling and theta connectivity. The two atypical APDs, but not the classical APD haloperidol, reduced prefrontal and cortical-hippocampal hypersynchrony produced by PCP. In fact, haloperidol exacerbated the hypersynchronization, including prefrontal fast delta, fast delta-HFO coupling and hippocampal high gamma oscillations. Notably, clozapine was the only drug that fully rescued the directionality of signals within the circuit, which is a crucial point considering that disrupted circuit communication is considered to be a hallmark of schizophrenia (Godsil et al. 2013; Hunt et al. 2017).

The fast delta rhythms observed after the administration of PCP support the proposed mechanism of a large-scale delta connectivity in schizophrenia resulting from an excessive thalamo-cortical delta drive (Hunt and Kasicki 2013; Hunt et al. 2017). Brain-wide aberrant delta activity is commonly found in patients with schizophrenia during wakefulness (Siekmeier and Stufflebeam 2010), for example, interhemispheric delta coupling is present during hallucinations (Spencer et al. 2009). Delta oscillations in the cortex arise from intrinsically bursting layer 5 pyramidal cells that are mediated between $GABA_B$ receptor inhibition and recurrent excitation (Hunt et al. 2017). Therefore, excessive delta power may be a biomarker of disinhibition of pyramidal neurons due to NMDAR hypofunction in GABAergic interneurons.

Fast delta synchronization produced by PCP entrained abnormal network activities at high gamma and HFOs, consequently boosting their power, cross-frequency coupling, spike-LFP coupling and circuit coherence. Cortical gamma increases emerge during psychosis in healthy individuals and patients diagnosed with schizophrenia and are subsequently recovered by APDs (Uhlhaas and Singer 2010; Jones et al. 2012; Shaw et al. 2015). In rodents, NMDAR antagonists also increase gamma oscillations in cortical regions and this increase can also be rescued by APDs (Phillips et al. 2012; Caixeta et al. 2013; Ahnaou et

al. 2017; Hunt et al. 2017). We found that risperidone, clozapine and the serotonergic agents reduced PCP-amplified prefrontal high gamma power, while haloperidol did not. This finding suggests that 5-HT_{2A}R antagonism and 5-HT_{1A}R agonism play causal roles in atypical APD's ability to attenuate aberrant cortical gamma power. HFOs (>100 Hz) have been investigated in humans in the context of epilepsy but much less in psychosis, likely due to the technical limitations of detecting HFOs by scalp EEG and MEG (Zijlmans et al. 2012). So, an association between psychosis and HFOs still needs to be established at a clinical level. Intracerebral recordings in rodents show that the NMDAR antagonists, PCP and ketamine, produce substantial increases in the power of HFOs and HFO coupling with delta waves in several brain regions including cortical areas, the HPC, and the nucleus accumbens (Flores et al. 2015; Hunt et al. 2015, 2017; Pittman-Polletta et al. 2018). Previous studies have shown that mesolimbic theta and delta oscillations that modulate HFO amplitude are driven by rhythmic activity generated in HPC and PFC, respectively, in which both compete for the control of the circuit (Pittman-Polletta et al. 2018). Accordingly, we also found that PCP produced significant increases in prefrontal HFO power and coupling of HFOs with delta oscillations, which were subsequently reduced by risperidone but not by haloperidol or clozapine. Additionally, M100907 and 8-OH-DPAT rescued PCP-induced HFOs, which suggests that 5-HT_{2A}R antagonism and 5-HT_{1A}R agonism mediate risperidone's ability to reduce prefrontal HFOs.

Previous studies suggest that abnormal activity of parvalbumin-expressing (PV+) interneurons may be responsible for the increase of gamma oscillations in schizophrenia. In support of this, postmortem studies of schizophrenia patients report reduced GABA synthesis in PV+ neurons (Gonzalez-Burgos et al. 2015). Moreover, mice lacking NMDARs on PV+ neurons have increased spontaneous gamma power in the HPC and cortex (Korotkova et al. 2010; Carlén et al. 2012; Guyon et al. 2021). Therefore, in our study the blockade of NMDARs in PV+ neurons by PCP may have been critically involved in the amplification of high gamma oscillations. Importantly, different subpopulations of PV+ neurons in the PFC express 5-HT_{1A}R and 5-HT_{2A}R (Puig et al. 2010), rendering these neurons key elements in the gamma reduction mediated by atypical APDs. In contrast, the neural mechanisms underlying PCP-mediated HFO are not

clear. A recent study has found a close correlation between the firing rates of PV+ neurons and HFOs in the medial PFC of healthy animals, although a causal relationship could not be established (Yao et al. 2020). Moreover, local blockade of NMDARs in the nucleus accumbens increases the power of HFOs (Hunt et al. 2010), although the neurons involved in generating these HFOs are unknown. Thus, the exact neural mechanisms underlying HFOs emerging during psychosis and their response to APDs will need further investigation.

None of the drugs reinstated hippocampal theta oscillations, theta-gamma coupling, and theta-beta circuit coherence. Since only risperidone and M100907 sedated the animals, decreased mobility associated with sedation was not a main contributor to the inability of APDs to rescue PCP-induced suppression of neural activities. Discoordination of hippocampal network activities by PCP has been associated with spatial cognitive impairment (Kao et al. 2017). Therefore, because neither haloperidol nor the atypical APDs restored network activity in the hippocampus, it may be that these APDs cannot rescue facets of cognition impaired by PCP.

Our results demonstrate that 5-HT_{2A}R antagonism and 5-HT_{1A}R agonism exert strong influences on prefrontal-hippocampal pathways under psychotic-like states and suggest that they likely contributed to the actions of risperidone and clozapine. In particular, the way in which the 5-HT_{2A}R antagonist, M100907, and risperidone blocked PCP's actions appeared to be similar, which likely reflects risperidone's strong affinity for 5-HT_{2A}Rs. Conversely, D2R antagonism by haloperidol produced little changes on the circuit's neural dynamics. This suggests that atypical APDs, but not typical APDs, target prefrontal-hippocampal pathways to elicit antipsychotic action. It is important to note that other brain areas including the thalamus and the nucleus accumbens likely contributed to the antipsychotic effects of risperidone and clozapine. Our findings underscore that understanding how APDs affect brain circuit dynamics in animal models, even assuming the unavoidable limitations of the models, may prove useful to gain insight into the pathophysiology of schizophrenia and advance the development of novel therapeutic interventions.

In conclusion, risperidone, and clozapine, but not haloperidol, reduced PCP-induced prefrontal and circuit hypersynchronization, which may point to a fundamentally different neural mechanism by which atypical APDs and typical APDs treat the core positive, negative and cognitive symptoms in schizophrenia. These differential effects likely reflect the different affinity of atypical APDs and haloperidol for serotonin and dopamine receptors.

CONFLICT OF INTEREST

The authors declare no conflict of interest.

ACKNOWLEDGMENTS

We thank Patricia Robledo for advice on the behavioral effects of PCP, Javier Zorrilla de San Martín for providing the PPC script, and Oriol Julve for support in video editing. This work was funded by the Spanish Agencia Estatal de Investigación (AEI/FEDER, UE; grant numbers SAF2016-80726-R, PID2019-104683RB-I00), Generalitat de Catalunya AGAUR (grant number 2018 FI_B_00112 to CD-S), and the Spain-USA Fulbright program (to ABF).

AUTHOR CONTRIBUTIONS

CDS, TG and MVP designed research; CDS, TG, MT and ABF performed research; CDS, PN, ABF and MVP analyzed data; all the authors wrote the paper.

REFERENCES

Ahnaou A, Huysmans H, Van de Casteele T, Drinkenburg WHIM. 2017. Cortical high gamma network oscillations and connectivity: a translational index for antipsychotics to normalize aberrant neurophysiological activity. Transl Psychiatry. 7:1285–1285.

Alemany-González M, Gener T, Nebot P, Vilademunt M, Dierssen M, Puig MV. 2020. Prefrontal-hippocampal functional connectivity encodes recognition memory and is impaired in intellectual disability. Proc Natl Acad Sci. 117:11788–11798.

Baker JT, Holmes AJ, Masters GA, Thomas Yeo BT, Krienen F, Buckner RL, Öngür D. 2014. Disruption

of Cortical Association Networks in Schizophrenia and Psychotic Bipolar Disorder. JAMA Psychiatry. 71:109–118.
Benetti S, Mechelli A, Picchioni M, Broome M, Williams S, McGuire P. 2009. Functional integration between the posterior hippocampus and prefrontal cortex is impaired in both first episode schizophrenia and the at risk mental state. Brain J Neurol. 132:2426–2436.
Berumen LC, Rodríguez A, Miledi R, García-Alcocer G. 2012. Serotonin receptors in hippocampus. Sci World J. 2012.
Caixeta FV, Cornélio AM, Scheffer-Teixeira R, Ribeiro S, Tort ABL. 2013. Ketamine alters oscillatory coupling in the hippocampus. Sci Rep. 3:2348.
Carlén M, Meletis K, Siegle JH, Cardin JA, Futai K, Vierling-Claassen D, Rühlmann C, Jones SR, Deisseroth K, Sheng M, Moore CI, Tsai L-H. 2012. A critical role for NMDA receptors in parvalbumin interneurons for gamma rhythm induction and behavior. Mol Psychiatry. 17:537–548.
Castañé A, Santana N, Artigas F. 2015. PCP-based mice models of schizophrenia: differential behavioral, neurochemical and cellular effects of acute and subchronic treatments. Psychopharmacology (Berl). 232:4085–4097.
Celada P, Puig MV, Artigas F. 2013. Serotonin modulation of cortical neurons and networks. Front Integr Neurosci.
Colgin LL. 2015. Do slow and fast gamma rhythms correspond to distinct functional states in the hippocampal network? Brain Res. 1621:309–315.
Flores FJ, Ching S, Hartnack K, Fath AB, Purdon PL, Wilson MA, Brown EN. 2015. A PK-PD model of ketamine-induced high-frequency oscillations. J Neural Eng. 12:056006.
Gener T, Tauste Campo A, Alemany-González M, Nebot P, Delgado-Sallent C, Chanovas J, Puig MV. 2019. Serotonin 5-HT1A, 5-HT2A and dopamine D2 receptors strongly influence prefronto-hippocampal neural networks in alert mice: Contribution to the actions of risperidone. Neuropharmacology. 158:107743–107743.
Godsil BP, Kiss JP, Spedding M, Jay TM. 2013. The hippocampal–prefrontal pathway: The weak link in psychiatric disorders? Eur Neuropsychopharmacol. 23:1165–1181.
Gonzalez-Burgos G, Cho RY, Lewis DA. 2015. Alterations in cortical network oscillations and parvalbumin neurons in schizophrenia. Biol Psychiatry. 77:1031–1040.
Grayson B, Idris NF, Neill JC. 2007. Atypical antipsychotics attenuate a sub-chronic PCP-induced cognitive deficit in the novel object recognition task in the rat. Behav Brain Res. 184:31–38.
Grützner C, Wibral M, Sun L, Rivolta D, Singer W, Maurer K, Uhlhaas PJ. 2013. Deficits in high- (>60 Hz) gamma-band oscillations during visual processing in schizophrenia. Front Hum Neurosci. 7:88.
Guyon N, Zacharias LR, Oliveira EF de, Kim H, Leite JP, Lopes-Aguiar C, Carlén M. 2021. Network asynchrony underlying increased broadband gamma power. J Neurosci.
Hardmeier M, Hatz F, Bousleiman H, Schindler C, Stam CJ, Fuhr P. 2014. Reproducibility of functional connectivity and graph measures based on the phase lag index (PLI) and weighted phase lag index (wPLI) derived from high resolution EEG. PloS One. 9:e108648–e108648.
Heckers S, Konradi C. 2010. Hippocampal pathology in schizophrenia. In: Swerdlow NR, editor. Behavioral neurobiology of schizophrenia and its treatment. Heidelberg: Springer. p. 529–553.
Hentschke H, Perkins MG, Pearce RA, Banks MI. 2007. Muscarinic blockade weakens interaction of gamma with theta rhythms in mouse hippocampus. Eur J Neurosci. 26:1642–1656.
Houthoofd SAMK, Morrens M, Sabbe BGC. 2008. Cognitive and psychomotor effects of risperidone in schizophrenia and schizoaffective disorder. Clin Ther. 30:1565–1589.
Hunt MJ, Falinska M, Łęski S, Wójcik DK, Kasicki S. 2010. Differential effects produced by ketamine on oscillatory activity recorded in the rat hippocampus, dorsal striatum and nucleus accumbens: J Psychopharmacol (Oxf).
Hunt MJ, Kasicki S. 2013. A systematic review of the effects of NMDA receptor antagonists on oscillatory activity recorded in vivo. J Psychopharmacol (Oxf). 27:972–986.

Hunt MJ, Kopell NJ, Traub RD, Whittington MA. 2017. Aberrant network activity in schizophrenia. Trends Neurosci. 40:371–382.
Hunt MJ, Olszewski M, Piasecka J, Whittington MA, Kasicki S. 2015. Effects of NMDA receptor antagonists and antipsychotics on high frequency oscillations recorded in the nucleus accumbens of freely moving mice. Psychopharmacology (Berl). 232:4525–4535.
Hunt MJ, Raynaud B, Garcia R. 2006. Ketamine dose-dependently induces high-frequency oscillations in the nucleus accumbens in freely moving rats. Biol Psychiatry. 60:1206–1214.
Jensen O, Colgin LL. 2007. Cross-frequency coupling between neuronal oscillations. Trends Cogn Sci. 11:267–269.
Jodo E. 2013. The role of the hippocampo-prefrontal cortex system in phencyclidine-induced psychosis: a model for schizophrenia. J Physiol Paris. 107:434–440.
Jones NC, Reddy M, Anderson P, Salzberg MR, O'Brien TJ, Pinault D. 2012. Acute administration of typical and atypical antipsychotics reduces EEG γ power, but only the preclinical compound LY379268 reduces the ketamine-induced rise in γ power. Int J Neuropsychopharmacol. 15:657–668.
Kao H-Y, Dvořák D, Park E, Kenney J, Kelemen E, Fenton AA. 2017. Phencyclidine discoordinates hippocampal network activity but not place fields. J Neurosci. 37:12031–12049.
Korotkova T, Fuchs EC, Ponomarenko A, von Engelhardt J, Monyer H. 2010. NMDA receptor ablation on parvalbumin-positive interneurons impairs hippocampal synchrony, spatial representations, and working memory. Neuron. 68:557–569.
Krystal JH, Karper LP, Seibyl JP, Freeman GK, Delaney R, Bremner JD, Heninger GR, Bowers MB, Charney DS. 1994. Subanesthetic effects of the noncompetitive NMDA antagonist, ketamine, in humans. Psychotomimetic, perceptual, cognitive, and neuroendocrine responses. Arch Gen Psychiatry. 51:199–214.
Lahti AC, Koffel B, LaPorte D, Tamminga CA. 1995. Subanesthetic doses of ketamine stimulate psychosis in schizophrenia. Neuropsychopharmacol Off Publ Am Coll Neuropsychopharmacol. 13:9–19.
Lee J, Hudson MR, O'Brien TJ, Nithianantharajah J, Jones NC. 2017. Local NMDA receptor hypofunction evokes generalized effects on gamma and high-frequency oscillations and behavior. Neuroscience. 358:124–136.
Meltzer H, Massey B. 2011. The role of serotonin receptors in the action of atypical antipsychotic drugs. Curr Opin Pharmacol. 11:59–67.
Meltzer HY, Huang M. 2008. In vivo actions of atypical antipsychotic drug on serotonergic and dopaminergic systems. In: Serotonin and Dopamine Interaction: Experimental Evidence and Therapeutic Relevance. Elsevier. p. 177–197.
Meltzer HY, McGurk SR. 1999. The effects of clozapine, risperidone, and olanzapine on cognitive function in schizophrenia. Schizophr Bull. 25:233–256.
Minzenberg MJ, Laird AR, Thelen S, Carter CS, Glahn DC. 2009. Meta-analysis of 41 functional neuroimaging studies of executive function in schizophrenia. Arch Gen Psychiatry. 66:811–811.
Nandi B, Swiatek P, Kocsis B, Ding M. 2019. Inferring the direction of rhythmic neural transmission via inter-regional phase-amplitude coupling (ir-PAC). Sci Rep. 9:6933.
Neill JC, Barnes S, Cook S, Grayson B, Idris NF, McLean SL, Snigdha S, Rajagopal L, Harte MK. 2010. Animal models of cognitive dysfunction and negative symptoms of schizophrenia: focus on NMDA receptor antagonism. Pharmacol Ther. 128:419–432.
Nolte G, Ziehe A, Nikulin VV, Schlögl A, Krämer N, Brismar T, Müller K-R. 2008. Robustly estimating the flow direction of information in complex physical systems. Phys Rev Lett. 100:234101–234101.
Phillips KG, Cotel MC, McCarthy AP, Edgar DM, Tricklebank M, O'Neill MJ, Jones MW, Wafford KA. 2012. Differential effects of NMDA antagonists on high frequency and gamma EEG oscillations in a neurodevelopmental model of schizophrenia. Neuropharmacology, Schizophrenia. 62:1359–1370.

Pittman-Polletta B, Hu K, Kocsis B. 2018. Subunit-specific NMDAR antagonism dissociates schizophrenia subtype-relevant oscillopathies associated with frontal hypofunction and hippocampal hyperfunction. Sci Rep. 8:11588.
Puig MV, Gener T. 2015. Serotonin modulation of prefronto-hippocampal rhythms in health and disease. ACS Chem Neurosci. 6:1017–1025.
Puig MV, Gulledge AT. 2011. Serotonin and prefrontal cortex function: Neurons, networks, and circuits. Mol Neurobiol.
Puig MV, Watakabe A, Ushimaru M, Yamamori T, Kawaguchi Y. 2010. Serotonin modulates fast-spiking interneuron and synchronous activity in the rat prefrontal cortex through 5-HT1A and 5-HT2A receptors. J Neurosci. 30:2211–2222.
Puighermanal E, Biever A, Espallergues J, Gangarossa G, De Bundel D, Valjent E. 2015. drd2-cre:ribotag mouse line unravels the possible diversity of dopamine d2 receptor-expressing cells of the dorsal mouse hippocampus. Hippocampus. 25:858–875.
Santana N, Mengod G, Artigas F. 2009. Quantitative analysis of the expression of dopamine D1 and D2 receptors in pyramidal and GABAergic neurons of the rat prefrontal cortex. Cereb Cortex. 19:849–860.
Scheffer-Teixeira R, Tort ABL. 2017. Unveiling fast field oscillations through comodulation. eneuro.
Shaw AD, Saxena N, E. Jackson L, Hall JE, Singh KD, Muthukumaraswamy SD. 2015. Ketamine amplifies induced gamma frequency oscillations in the human cerebral cortex. Eur Neuropsychopharmacol. 25:1136–1146.
Siekmeier PJ, Stufflebeam SM. 2010. Patterns of spontaneous magnetoencephalographic activity in patients with schizophrenia. J Clin Neurophysiol Off Publ Am Electroencephalogr Soc. 27:179–190.
Sigurdsson T. 2016. Neural circuit dysfunction in schizophrenia: Insights from animal models. Neuroscience. 321:42–65.
Sigurdsson T, Duvarci S. 2016. Hippocampal-prefrontal interactions in cognition, behavior and psychiatric disease. Front Syst Neurosci. 9:190–190.
Sigurdsson T, Stark KL, Karayiorgou M, Gogos JA, Gordon JA. 2010. Impaired hippocampal-prefrontal synchrony in a genetic mouse model of schizophrenia. Nature. 464:763–767.
Spencer KM, Niznikiewicz MA, Nestor PG, Shenton ME, McCarley RW. 2009. Left auditory cortex gamma synchronization and auditory hallucination symptoms in schizophrenia. BMC Neurosci. 10:85.
Spencer KM, Salisbury DF, Shenton ME, McCarley RW. 2008. Gamma-band auditory steady-state responses are impaired in first episode psychosis. Biol Psychiatry. 64:369–375.
Stam CJ, Nolte G, Daffertshofer A. 2007. Phase lag index: assessment of functional connectivity from multi channel EEG and MEG with diminished bias from common sources. Hum Brain Mapp. 28:1178–1193.
Sturgeon RD, Fessler RG, Meltzer HY. 1979. Behavioral rating scales for assessing phencyclidine-induced locomotor activity, stereotyped behavior and ataxia in rats. Eur J Pharmacol. 59:169–179.
Tavares LC, Tort AB. 2020. Hippocampal-prefrontal interactions during spatial decision-making. bioRxiv. 2020.06.24.168732.
Tort ABL, Kramer MA, Thorn C, Gibson DJ, Kubota Y, Graybiel AM, Kopell NJ. 2008. Dynamic cross-frequency couplings of local field potential oscillations in rat striatum and hippocampus during performance of a T-maze task. Proc Natl Acad Sci U A. 105:20517–20522.
Uhlhaas PJ, Singer W. 2010. Abnormal neural oscillations and synchrony in schizophrenia. Nat Rev Neurosci. 11:100–113.
Vallat R. 2018. Pingouin: statistics in Python. J Open Source Softw. 3:1026.
Vinck M, Oostenveld R, Wingerden MV, Battaglia F, Pennartz CMA. 2011. An improved index of phase-synchronization for electrophysiological data in the presence of volume-conduction , noise and sample-size bias. NeuroImage. 55:1548–1565.

Yao Y, Wu M, Wang L, Lin L, Xu J. 2020. Phase coupled firing of prefrontal parvalbumin interneuron with high frequency oscillations. Front Cell Neurosci. 14:610741.
Zhang C, Li H, Han R. 2020. An open-source video tracking system for mouse locomotor activity analysis. BMC Res Notes. 13:48.
Zhang X, Zhong W, Brankačk J, Weyer SW, Müller UC, Tort ABL, Draguhn A. 2016. Impaired theta-gamma coupling in APP-deficient mice. Sci Rep. 1–10.
Zijlmans M, Jiruska P, Zelmann R, Leijten FSS, Jefferys JGR, Gotman J. 2012. High-Frequency Oscillations as a New Biomarker in Epilepsy. Ann Neurol. 71:169–178.
Zorrilla de San Martin J, Donato C, Peixoto J, Aguirre A, Choudhary V, De Stasi AM, Lourenço J, Potier M-C, Bacci A. 2020. Alterations of specific cortical GABAergic circuits underlie abnormal network activity in a mouse model of Down syndrome. eLife. 9:e58731.

FIGURES AND FIGURE LEGENDS

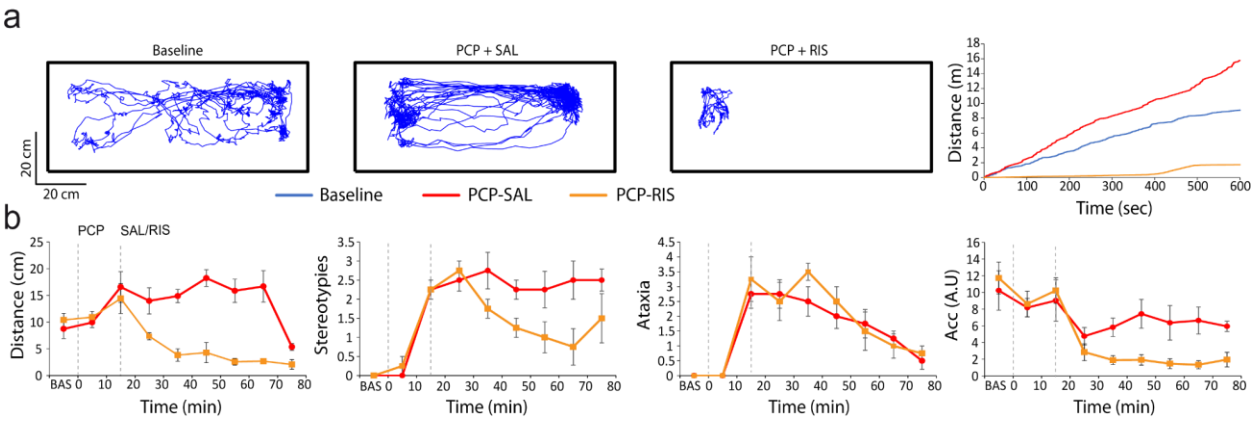

Figure 1: Acute PCP (10 mg/kg, SC) induced psychotic-like behavioral effects in mice. **(a)** Representative examples of 10-minute traces during baseline (left), after the administration of PCP+SAL (middle) and after the administration of PCP+RIS (0.5 mg/kg, IP; right) in one mouse. Quantification of distance traveled is shown on the right for baseline (blue), PCP+SAL (red) and PCP+RIS (orange). **(b)** Quantification of distance traveled, stereotypes, ataxia, and accelerometer during 10-minute epochs after the PCP injection. The groups quantified are PCP+SAL (n = 4 mice, red) and PCP+RIS (n = 4 mice, orange).

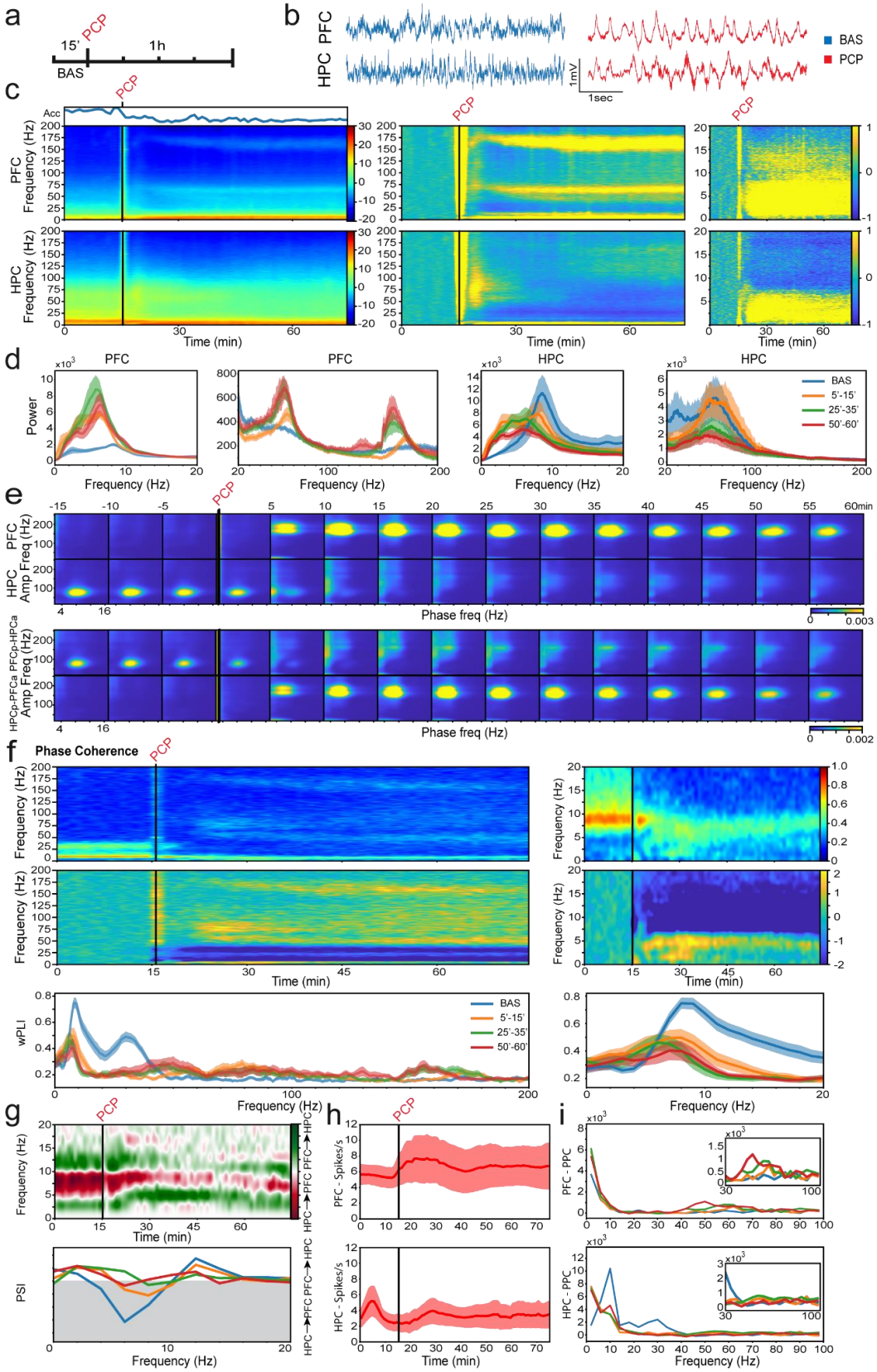
a
15'
PCP
1h
BAS
b
PFC
HPC
1mV
1sec
BAS
PCP
c
PCP
Acc
PFC Frequency (Hz)
HPC Frequency (Hz)
Time (min)
d
PFC
HPC
Power
Frequency (Hz)
BAS
5'-15'
25'-35'
50'-60'
e
PCP
PFC Freq (Hz)
HPC Amp Freq (Hz)
Phase freq (Hz)
HPCp-PFCa
PFCp-HPCa
f
Phase Coherence
PCP
Frequency (Hz)
Time (min)
wPLI
BAS
5'-15'
25'-35'
50'-60'
g
PCP
Frequency (Hz)
Time (min)
PSI
PFC→HPC
HPC→PFC
h
PCP
PFC - Spikes/s
HPC - Spikes/s
Time (min)
i
PFC - PPC
HPC - PPC
Frequency (Hz)

Figure 2: Acute administration of PCP boosts prefrontal synchronization, desynchronizes hippocampal microcircuits and disrupts circuit connectivity. **(a)** Experimental protocol. Recording LFP signals in freely moving mice during baseline conditions (BAS) for 15 minutes and for 1 hour following the administration of PCP (10 mg/kg, SC; n = 9 mice). **(b)** Representative examples of 5-second LFP traces recorded in the PFC and the HPC during baseline (blue) and after the administration of PCP (red) in one mouse. **(c)** Averaged spectrograms of signals in the PFC and the HPC. Left panels represent the raw data with the corresponding quantification of the animals' mobility (Acc, variance of signals from the accelerometer integrated within the headstages); middle and right panels represent the z-scores relative to baseline. The Acc results are presented as a ratio to the highest value in the baseline condition. **(d)** Power spectra of PFC and HPC signals during baseline (blue), 5 to 15 min (orange), 25 to 35 min (green) and 50 to 60 minutes (red) after the administration of PCP. The plots have been divided into 0-20 Hz and 20-200 Hz to facilitate the comparison. **(e)** Comodulation maps quantifying local and inter-regional cross-frequency coupling in consecutive non-overlapping 5-min epochs. The x-axis represents phase frequencies (2-16 Hz) and the y-axis represents amplitude frequencies (10-250 Hz). Numbers on top of the panels indicate the minute after PCP administration. (Top) Local modulation index in the PFC and the HPC. (Bottom) Inter-regional modulation index between the PFC phase (PFCp) and the HPC amplitude (HPCa) and between the HPC phase (HPCp) and the PFC amplitude (PFCa). **(f)** Time course of changes in phase coherence estimated with the weighted phase lag index (wPLI). Top panels represent the raw wPLI while the corresponding z-scores are shown below. Quantification of wPLI is shown on the lower panels. **(g)** Time course of changes in circuit directionality estimated with the phase slope index (PSI). HPC-to-PFC directionality is represented in red and PFC-to-HPC directionality in green. A simplified representation is shown below where the shaded area indicates HPC-to-PFC directionality. (h) Time course of changes in the firing rate of individual neurons in each brain area (20 and 15 neurons from 5 mice, respectively). (i) Spike-LFP coherence estimated with pairwise phase consistency (PPC). Multi-unit activity (MUA) was used in this analysis.

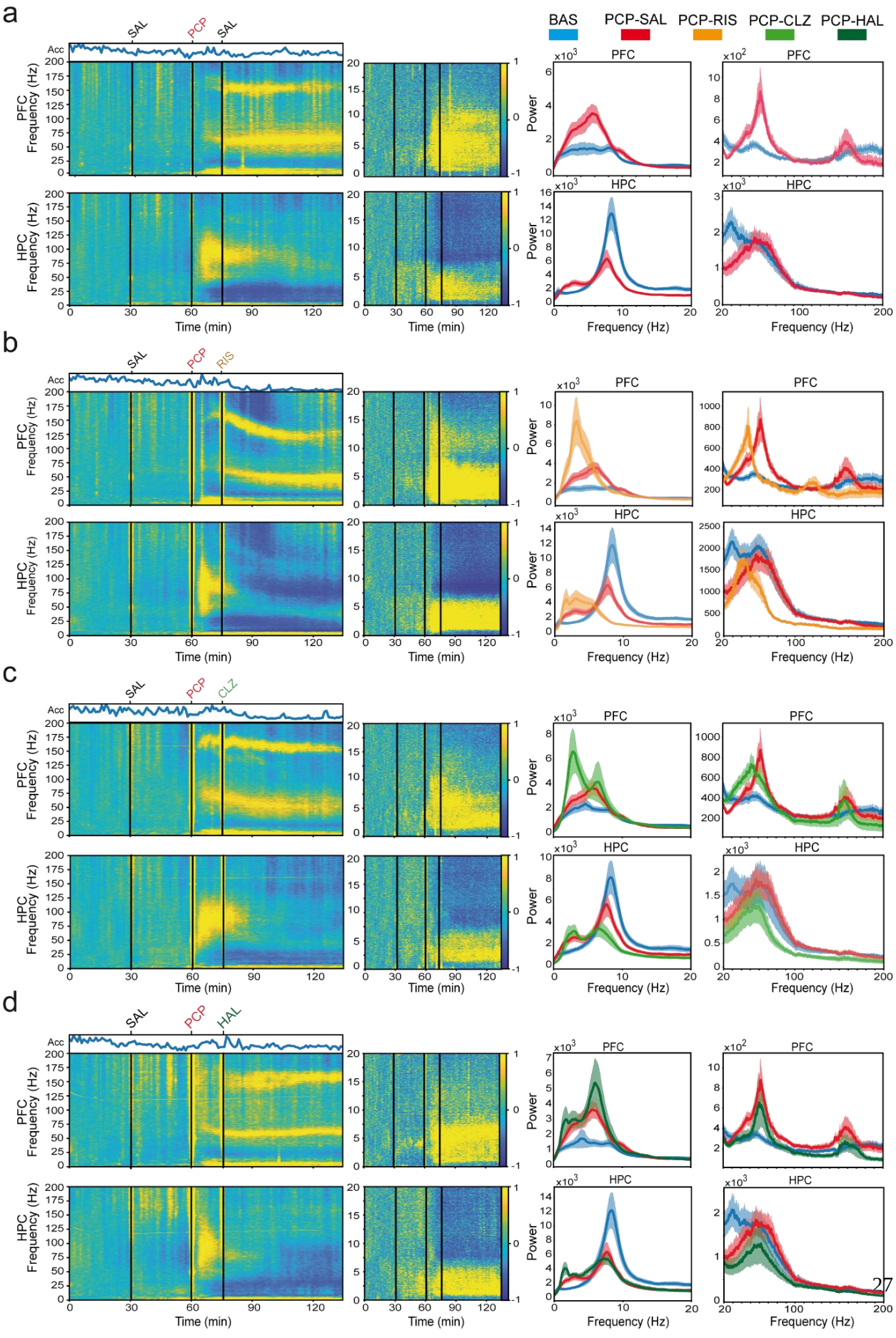
a
b
c
d
SAL
PCP
RIS
CLZ
HAL
Acc
PFC Frequency (Hz)
HPC Frequency (Hz)
Time (min)
BAS
PCP-SAL
PCP-RIS
PCP-CLZ
PCP-HAL
PFC
HPC
Power
Frequency (Hz)

Figure 3: Effects of saline (SAL, IP; n = 6 mice), risperidone (RIS, 0.5 mg/kg, IP; n = 7 mice), clozapine (CLZ, 1 mg/kg, IP; n = 6 mice) and haloperidol (HAL, 0.5 mg/kg, IP; n = 5 mice) on the local power in the PFC and HPC after acute PCP. All panels depict normalized spectrograms of the neural signals with respect to baseline (z-scores). The corresponding quantification of the animals' mobility (Acc) is shown above. The Acc results are presented as a ratio to the highest value in the baseline condition. Power spectra of the signals are shown on the right. The plots have been divided into 0-20 Hz and 20-200 Hz to facilitate the visualization.

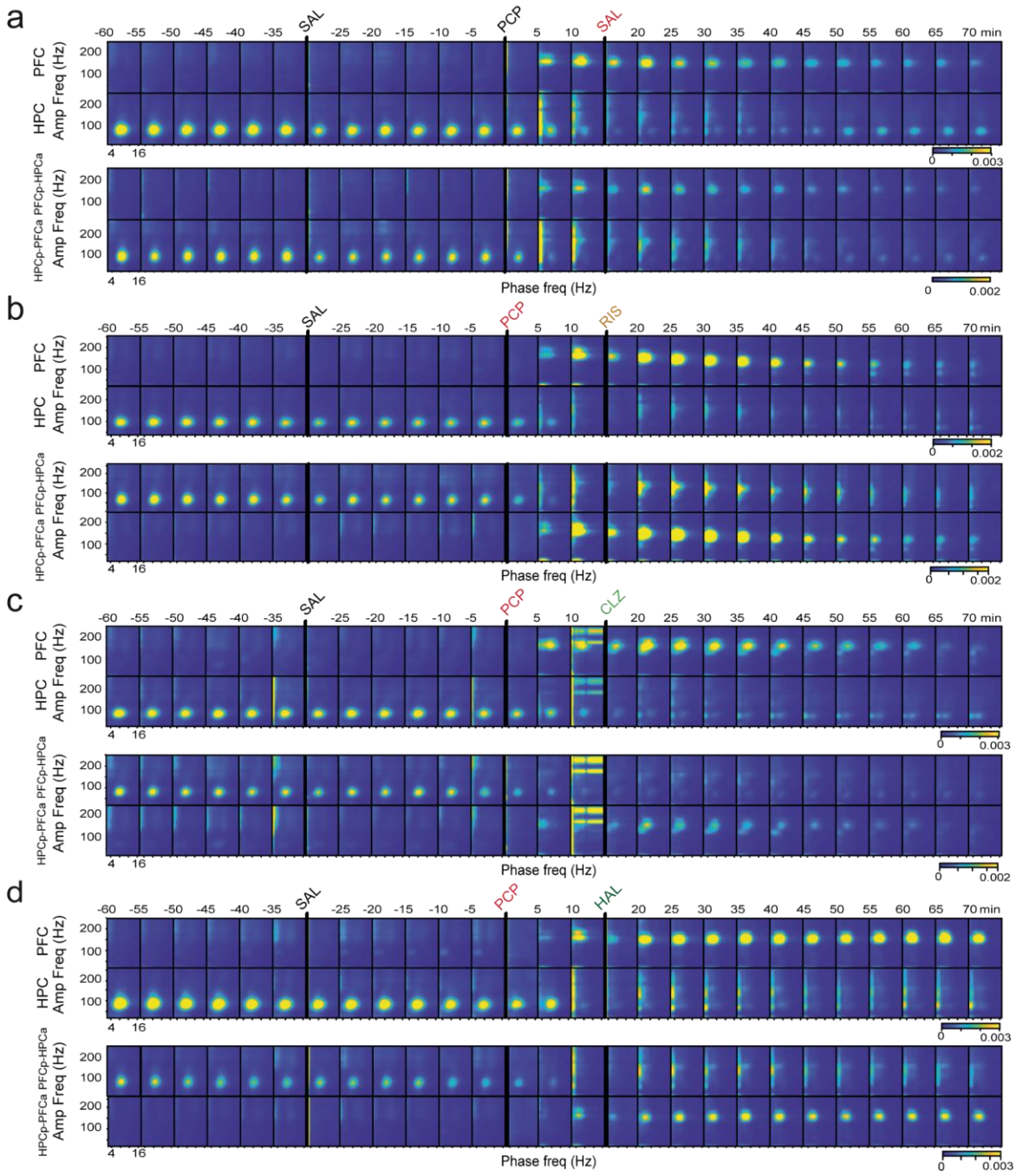

Figure 4: Effects of saline (SAL), risperidone (RIS), clozapine (CLZ) and haloperidol (HAL) on the local and inter-regional phase-amplitude cross-frequency coupling after acute PCP. All panels present comodulation maps quantifying local and inter-regional coupling in consecutive non-overlapping 5-min epochs. The numbers on top of the panels indicate the time after PCP administration. The upper panels show the local course of changes in the modulation index, while the lower panels show the inter-regional, PFC-phase HPC-amplitude and HPC-phase and PFC-amplitude coupling.

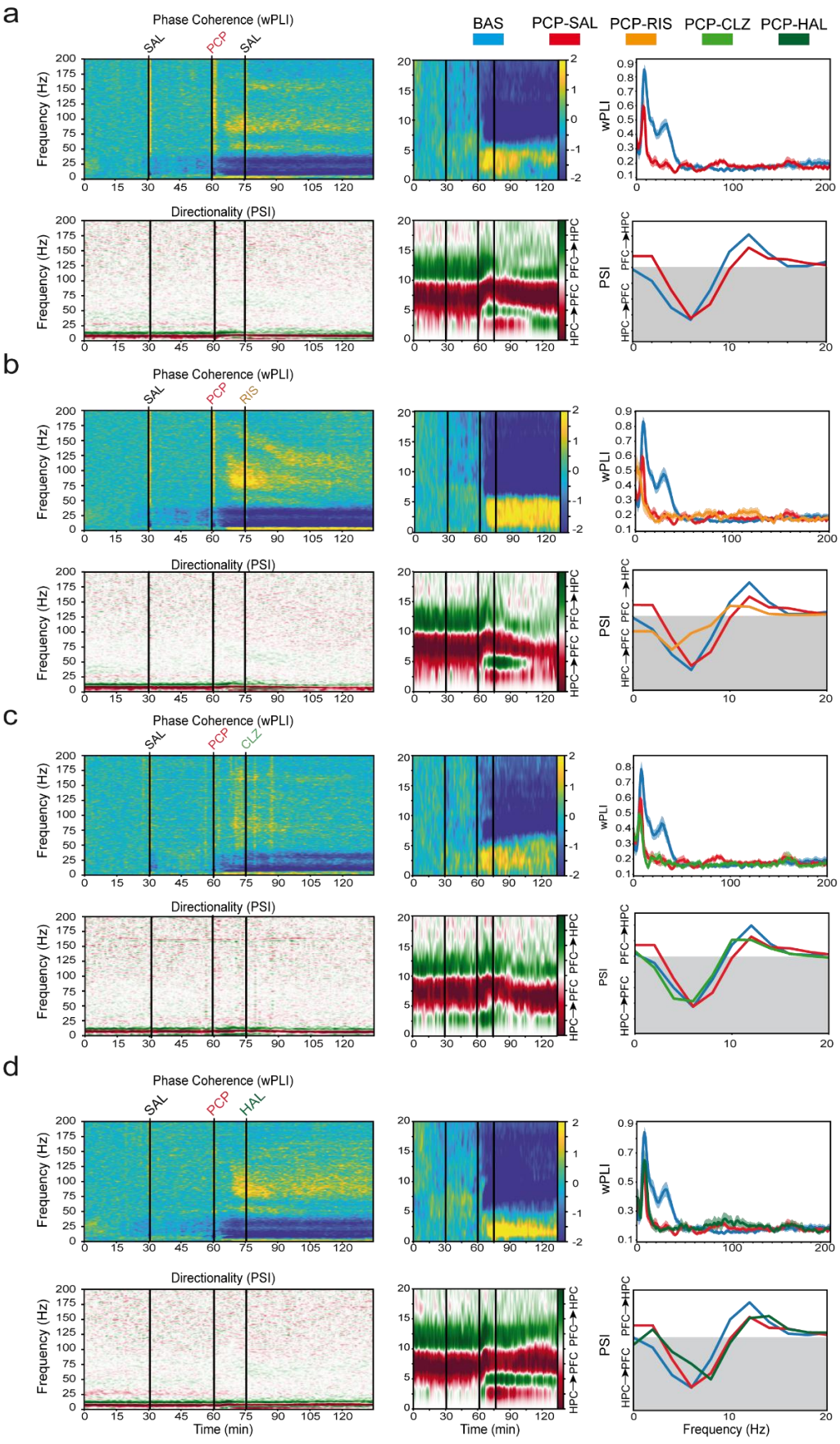
a
b
c
d
Phase Coherence (wPLI)
Directionality (PSI)
SAL
PCP
RIS
CLZ
HAL
BAS
PCP-SAL
PCP-RIS
PCP-CLZ
PCP-HAL
Frequency (Hz)
wPLI
PSI
HPC→PFC
PFC→HPC
Time (min)
Frequency (Hz)

Figure 5: Effects of saline (SAL), risperidone (RIS), clozapine (CLZ) and haloperidol (HAL) on prefrontal-hippocampal connectivity after acute PCP. All panels present a normalized (z-scores) time course of changes in wPLI (phase coherence) and corresponding quantification (right panels panels). The lower panels show the time course of changes in PSI (circuit signal directionality) and corresponding quantification. The shaded area represents hippocampus-to-cortex signal directionality, the line denoting zero PSI.

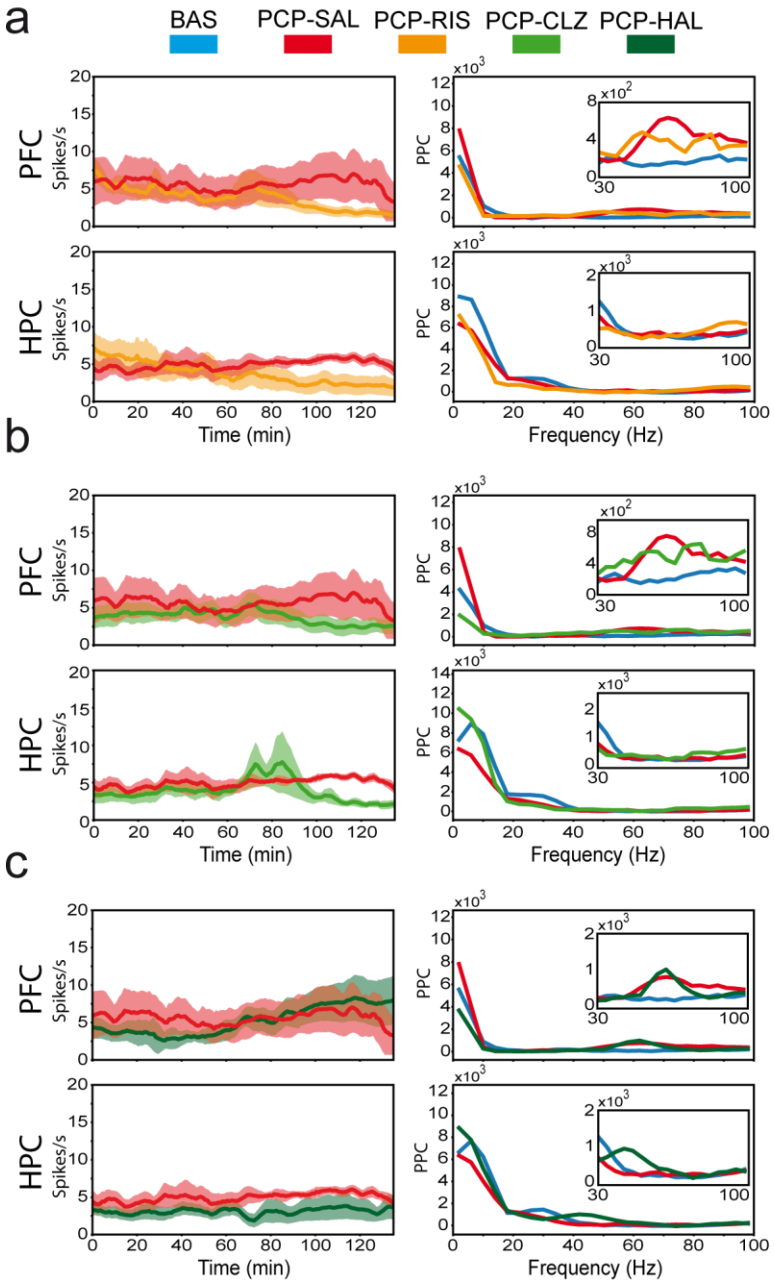

Figure 6: Effects of saline (SAL), risperidone (RIS), clozapine (CLZ) and haloperidol (HAL) on the firing rate of neurons and spike-LFP coupling after acute PCP. Left panels: Time course of changes in the firing rate of individual neurons (SUA) in each brain area (PCP+SAL: 6 and 7 neurons from 4 mice; PCP+RIS: 11 and 9 neurons from 4 mice; PCP+CLZ: 11 and 12 neurons from 4 mice; PCP+HAL: 9 and 10 neurons from 4 mice). Right panels: Spike-LFP coupling estimated with pairwise phase consistency (PPC). Multi-unit activity (MUA) was used in these analyses.

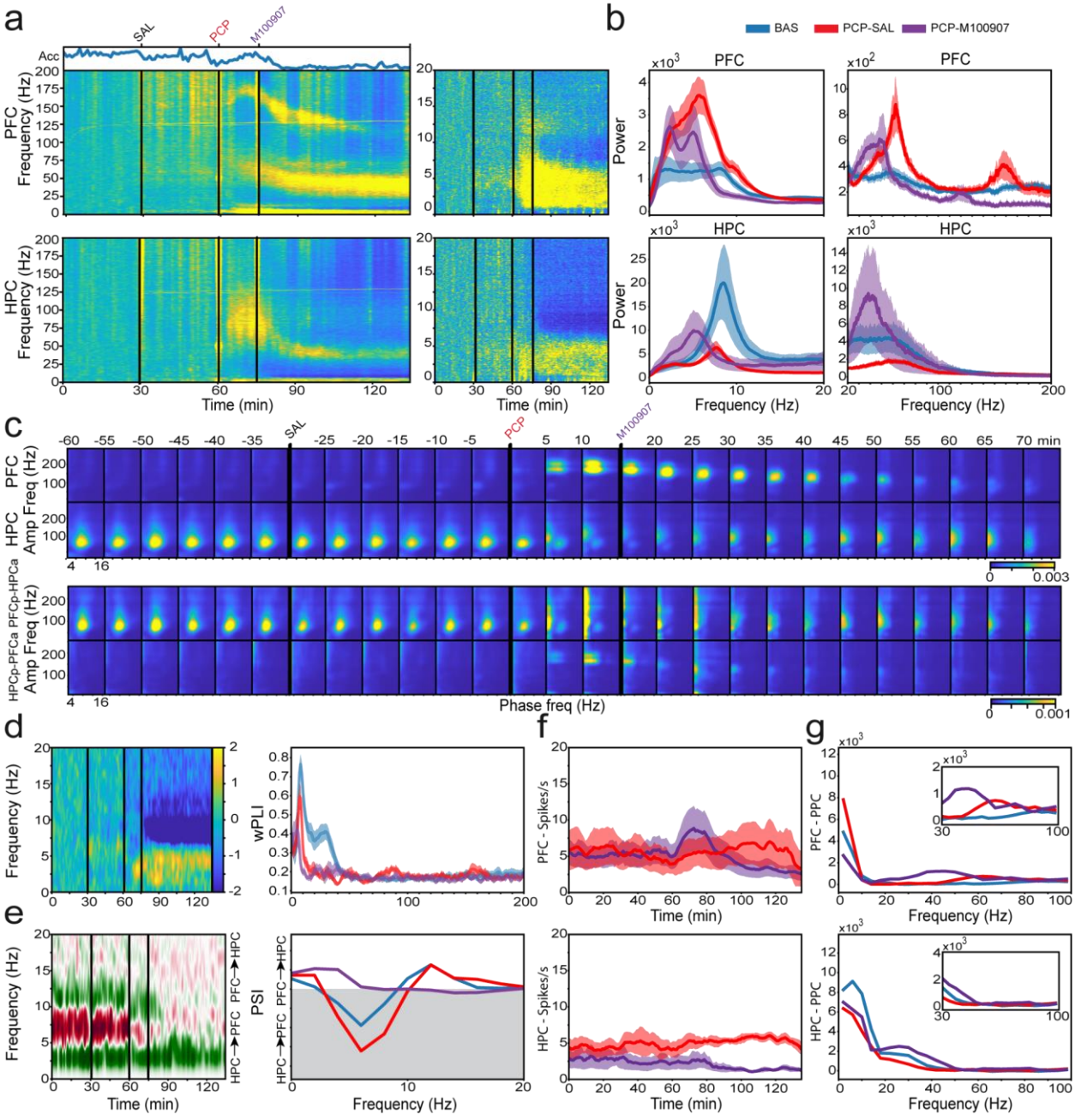
a
SAL
PCP
M100907
Acc
PFC Frequency (Hz)
HPC Frequency (Hz)
Time (min)
b
BAS
PCP-SAL
PCP-M100907
PFC
HPC
Power
Frequency (Hz)
c
PFC Amp Freq (Hz)
HPC Amp Freq (Hz)
HPCp-PFCa PFCp-HPCa Amp Freq (Hz)
Phase freq (Hz)
d
Frequency (Hz)
wPLI
e
PSI
PFC→HPC
HPC→PFC
f
PFC - Spikes/s
HPC - Spikes/s
Time (min)
g
PFC - PPC
HPC - PPC
Frequency (Hz)

Figure 7: M100907 (5-HT_{2A}R antagonist; 1 mg/kg, IP; n = 6 mice) reduced many PCP-induced alterations of prefrontal-hippocampal neural dynamics. **(a)** Normalized spectrograms (z-scores) of signals in the PFC (upper panels) and HPC (lower panels). The corresponding quantification of the animals' mobility (Acc) is also shown. The Acc results are presented as a ratio to the highest value in the baseline condition. **(b)** The power spectra of PFC and HPC signals during 10 min of baseline are represented in blue and signals from min 35 to 45 after M100907 (50-60 min after PCP) are illustrated in purple. Power spectra of signals recorded from min 35 to 45 after saline administration (50-60 min after PCP) are shown in red for comparison. **(c)** Comodulation maps quantifying local and inter-regional cross-frequency coupling in consecutive non-overlapping 5-min epochs. The numbers on top of the panels indicate time after PCP administration. **(d)** Normalized (z-scores) time course of changes in wPLI (phase coherence) and corresponding quantification. **(e)** Time course of changes in PSI (circuit directionality) and corresponding quantification. As above, the shaded area represents hippocampus-to-cortex directionality, the line denoting zero PSI. **(f)** Time course of changes in the firing rate of individual neurons (SUA) in each brain area (16 and 13 neurons from 5 mice, respectively). **(g)** Spike-LFP coupling estimated with pairwise phase consistency (PPC). Multi-unit activity (MUA) was used in these analyses.

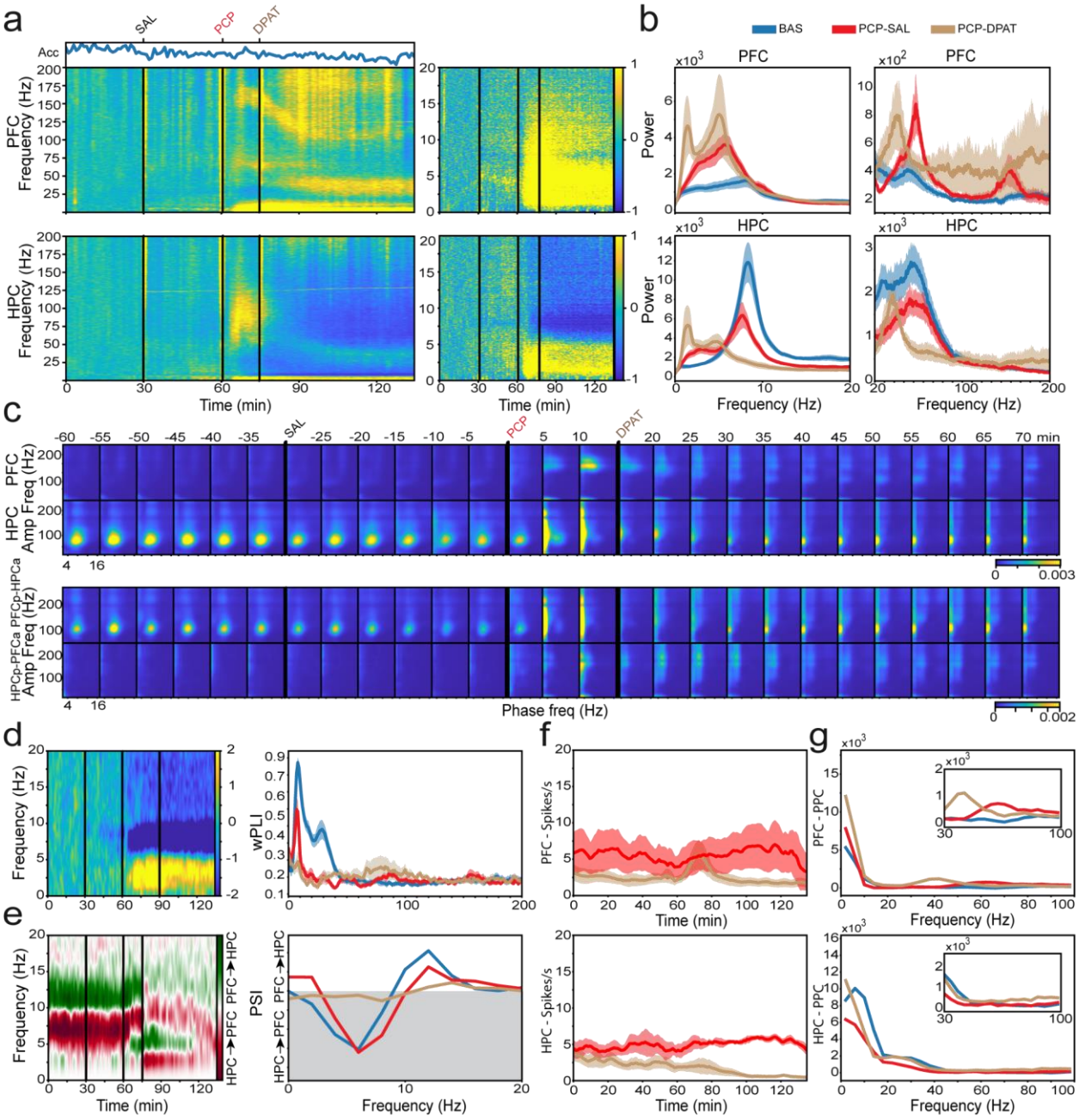

Figure 8: 8-OH-DPAT (DPAT, 5-HT$_{1A}$R agonist; 1 mg/kg, IP; n = 6 mice) reverses different PCP-induced alterations of prefrontal-hippocampal neural dynamics. **(a)**. Normalized spectrograms (z-scores) of signals in the PFC (upper panels) and HPC (lower panels). The corresponding quantification of the animals' mobility (Acc) is also shown. The Acc results are presented as a ratio to the highest value in the baseline condition. **(b)** The power spectra of PFC and HPC signals during 10 min of baseline are represented in blue and signals from min 35 to 45 DPAT administration (50-60 min after PCP) are illustrated in tan, respectively. Consistent with the previous figure, an additional group with power spectra of signals recorded

50-60 minutes after the administration of PCP-saline are shown in red for comparison. **(c)** Comodulation maps quantifying local and inter-regional cross-frequency coupling in consecutive non-overlapping 5-min epochs. The numbers on top of the panels indicate time after PCP administration. **(d)** Normalized (z-scores) time course of changes in wPLI (phase coherence) and corresponding quantification. **(e)** Time course of changes in PSI (circuit directionality) and corresponding quantification. The shaded area represents hippocampus-to-cortex directionality, the line denoting zero PSI. **(f)** Time course of changes in the firing rate of individual neurons (SUA) in each brain area (18 and 15 neurons from 5 mice, respectively). **(g)** Spike-LFP coupling estimated with pairwise phase consistency (PPC). Multi-unit activity (MUA) was used in these analyses.